Hard Spheres in Vesicles: Curvature-Induced Forces and Particle-Induced Curvature

A. D. Dinsmore, D. T. Wong, Philip Nelson, A. G. Yodh
Department of Physics and Astronomy
University of Pennsylvania
Philadelphia, PA 19104 U.S.A.
(July 8, 1997)

PACS numbers: 05.20.-y, 82.65.Dp, 82.70.Dd, 87.22.Bt.

We explore the interplay of membrane curvature and nonspecific binding due to excluded-volume effects among colloidal particles inside lipid bilayer vesicles. We trapped submicron spheres of two different sizes inside a pear-shaped, multilamellar vesicle and found the larger spheres to be pinned to the vesicle's surface and pushed in the direction of increasing curvature. A simple model predicts that hard spheres can induce shape changes in flexible vesicles. The results demonstrate an important relationship between the shape of a vesicle or pore and the arrangement of particles within it.

Entropic excluded-volume (depletion) effects are well known to lead to phase separation in the bulk of colloids and emulsions consisting of large and small particles with short-range repulsive interactions [1–6]. More recently, attraction of the large particles to flat, hard walls [7,8] and repulsion from step edges [9] have been demonstrated in binary hard-sphere mixtures. A key concept suggested in these papers is that the geometric features of the surface can create "entropic force fields" that trap, repel or induce drift of the larger particles. This mechanism is not limited to suspensions of micron-sized particles; it may play a role in "lock and key" steric interactions on smaller macromolecular length scales. For example, the shape of pores and liposomes inside cells is likely to affect the behavior of macromolecules confined within them [10].

In this Letter, we present experimental results that demonstrate new entropic effects at surfaces. In particular, the behavior of particles confined within vesicles reveals quantitatively the striking effect of membrane curvature. We first discuss experiments probing the behavior of a microscopic sphere trapped inside a rigid, phospholipid vesicle. Adding much smaller spheres to the mixture changes the distribution of the larger sphere in a way that depends on the curvature of the vesicle wall (see Fig. 1(b) and (c)). The results are consistent with the depletion force theory and illustrate a new mechanism for the size-dependent arrangement of particles within pores. We then explore theoretically some consequences of replacing the rigid wall with a flexible one. The entropic curvature effects can overcome the membrane's stiffness, leading to a new mechanism for shape changes in vesicles.

We first briefly review depletion effects in mixtures of microscopic hard spheres of two different sizes. Moving two of the larger spheres toward one another does not change their interaction energy (which is zero for hard spheres) but does increase the volume accessible to the other particles (Fig. 2). The resulting gain in entropy reduces the free energy of the system by $(3/2)\alpha\phi_S k_{\rm B}T$ [11,12]. Here, α is the ratio of large to small radii (R_L/R_S), ϕ_S is the small-sphere volume fraction, and $k_{\rm B}T$ is Boltzmann's constant times the absolute temperature. This simple result relies on the approximation that the small spheres are a structureless ideal gas and that the large-sphere volume fraction, ϕ_L, is small. The reduction of free energy produces an "entropic force" that pushes the large spheres together. When the large sphere is moved to a flat wall, moreover, the overlap volume and the free-energy loss are approximately doubled [7]. In binary hard-sphere mixtures, these effects are known to drive crystallization of large spheres in the bulk [1,2,5] and at a flat surface [1,7,13,14]. Furthermore, the shape of the wall can lead to entropic forces in a specific direction *along the wall*. For example, the larger spheres are locally repelled from an edge cut into the wall [9] and attracted to a corner (*i.e.* where the "wall" meets the "floor") [15]. If the wall has constantly-changing radius of curvature, these forces are predicted to act everywhere along it [9]. As shown in Fig. 2 (c), when the large sphere is near the wall, the overlap volume depends on the wall's curvature radius. The large sphere will therefore move in the direction of increasing curvature to minimize the small spheres' excluded volume.

To measure this surface entropic force, we have studied the distribution and dynamics of microscopic nearly-hard spheres trapped inside rigid, pear-shaped vesicles. The vesicles were prepared from a phospholipid (1-Stearoyl-2-Oleoyl-sn-Glycero-3-Phosphocholine (SOPC), Avanti Inc., U.S.A.), dissolved in chloroform (25 mg/mL). After evaporating the chloroform from 200 μL of SOPC solution, we added 100 μL of salt water with charge-stabilized polystyrene spheres (Seradyn, IN, USA) in suspension. The salt (0.01 M NaCl) served to screen out electrostatic forces over a distance of ≈ 5 nm, the Debye-Huckel screening length [7]. Thus, our sample closely resembled an ideal hard-sphere and hard-wall (HSHW) system. Rigid, multilamellar vesicles of diverse shapes and sizes immediately formed with colloidal spheres trapped inside. We injected the solution into a 10-μm thick glass container for viewing under an optical microscope (100x objective with 1.30 numerical aperture, in transmission mode). Images of a planar slice, 600 nm thick, through the center of vesicles were captured, then later digitized (Fig. 1(a)).

We quantified the behavior of the mixture by measuring its free energy, $F(\mathbf{r})$, as a function of the position of a sphere of radius $R_L = 0.237\,\mu$m. First, using NIH Image software, we determined the in-plane position of the sphere's center of mass, $\mathbf{r}$, ($\pm 0.08\mu$m) when it appeared in the imaged slice. From these data, we used two techniques to extract $F(\mathbf{r})$. In the first, the number of times $N(\mathbf{r}_i)$ the sphere appeared at a given bin located at $\mathbf{r}_i$ defined the density distribution. Assuming that each measurement event was independent of the others, $N(\mathbf{r}_i)$ follows the Boltzmann distribution: $N(\mathbf{r}_i) \propto \exp(-F(\mathbf{r}_i)/k_{\mathrm{B}}T)$. Since a systematic error can arise if events are not completely independent (*i.e.* not separated by an infinite time), we waited a minimum of 0.6 s between measurements. During this time the mean square displacement was $\approx 0.3\ \mu$m, larger than the 0.07-0.13 μm bin sizes. We also collected data over a period of 30-80 minutes, enough time for the sphere to explore all of the available space. We therefore used the logarithm of the sphere's distribution to extract the free energy.

The dynamics of the diffusing 0.237-μm sphere provided the second way to measure $F(\mathbf{r}_i)$, as described in [16]. The region along the inner surface of the vesicle was divided into several equal-area bins. We considered only events in which the center of the large sphere was within 0.28 μm of contact with the surface in consecutive frames (separated by a time τ). From our videotape, we counted the number of times ($N_{ij}(\tau)$) the sphere was located in bin j at time t and in bin i at time $t+\tau$. The transition probability matrix, $P_{ij}(\tau)$, is given by $N_{ij}(\tau)/N(\mathbf{r}_j)$. The measured matrix P_{ij} contains information about the equilibrium state of the system. In particular, the eigenvector ($\hat{\mathbf{e}}$) of P_{ij} with unit eigenvalue is proportional to the Boltzmann factor: $\hat{\mathbf{e}}_i \propto \exp(-F(\mathbf{r}_i)/k_{\mathrm{B}}T)$. We obtained consistent results with $\tau = 0.1$, 0.2 and 0.3 s and with various bin sizes. This technique avoids fit parameters and possible systematic errors arising from the density-distribution approach. It also avoids potential errors arising from a slow change in shape of the vesicle, which would affect the distribution averaged over a long time but would not affect the short-time particle dynamics. We report here the results from two different samples. The first "control" sample contained a solitary 0.237-μm sphere (no small spheres) diffusing freely inside a vesicle. The measured density distribution is shown in Fig. 1(b). The sphere distribution is uniform: there is no significant interaction between the vesicle wall and the polystyrene sphere, as expected due to the very short Debye-Huckel screening length.

The behavior changed noticeably when small spheres were added to the interior of a vesicle. In Fig. 1(c), we show the distribution of the $R_L = 0.237\,\mu$m sphere in a binary mixture with $\phi_S = 0.3, R_S = 0.042\mu$m ($\alpha = 5.7$). The distribution is highly non-uniform, with a significantly higher probability of finding the large sphere within about 0.28 μm of the surface. The apparent width of this "surface" region exceeds $2R_S$ due to uncertainties in the particle positions and, possibly, due to a slight tilt of the vesicle wall away from vertical.

We measured the average number of times the large sphere appeared in each bin within 0.28 μm of the surface and the average number per bin in the bulk. We defined the natural logarithm of the ratio of these numbers as $F_0/(k_B T)$, a measure of the average strength of the depletion attraction. We found $F_0 = (2.2 \pm 0.5)k_B T$.

Theoretically, $F_0 = \ln \int_{R_L}^{R_L + 0.28\ \mu\mathrm{m}} [\mathrm{d}r/0.28\ \mu\mathrm{m}]\, \mathrm{e}^{-V(r)/k_B T}$, where r is the distance from the large-sphere center to the wall and $V(r)$ is given by the depletion force model. Although the vesicle wall was curved, we can predict a lower bound of F_0 by assuming the wall is flat:

$$V(r) = \frac{-k_B T \phi_S}{4R_S^3}(r - R_L - 2R_S)^2(r + 2R_L + R_S). \quad (1)$$

Putting in the numbers gives a theoretical prediction of $F_0 = 1.97 k_B T$. Here we have neglected thermal fluctuations in the shape of the vesicle wall and residual electrostatic repulsion. Constraining the large sphere to lie 5 nm away from the wall, for example, reduces the predicted result to 1.45 $k_B T$. The 0.7-$k_B T$ difference from our measured result is likely due to the curvature of the wall, which would enhance the observed F_0 as discussed in the following paragraph. These results are consistent with recent calculations showing that the ideal-gas approximation accurately predicts the depletion well depth at contact (although it misses the relatively weak, long-range depletion repulsion) [17].

The distribution in Fig. 1(c) demonstrates a higher large-sphere occupation where the vesicle surface is more curved. ¿From the sphere dynamics, we obtained the total free energy, F, as a function of sphere position when it was near the surface. The inset of Fig. 3 shows the measured F as a function of the position, s, along the perimeter. The slope of this curve reveals a maximum force of 20x$10^{-15} N$ pushing the large sphere along the wall. We also determined the curvature radius at points along the wall using our images of the vesicle. In Fig. 3, we plot the free energy as a function of wall curvature radius, R_C. The free energy decreased by approximately $1.5 k_{\mathrm{B}} T$ when the curvature radius decreased from 20 μm to 2 μm. For comparison to our results, we used the simple depletion-force model described above (Fig. 2(c)) to calculate the free energy as a function of wall curvature (assuming a locally spherical wall): $F(R_C) = -P_S V_{\mathrm{overlap}}(R_C)$. Here, P_S is the small-particle osmotic pressure (from the ideal-gas law) and $V_{\mathrm{overlap}}(R_C)$ is the size of the excluded-volume overlap.

The large sphere was assumed to touch the vesicle wall. The theory, represented by the solid line in Fig. 3, is consistent with the experimental results. For both plots, the free energy was set to 0 in the limit of large curvature radius (flat wall). Since we could only measure R_C in the image plane, we assumed that this also determined the out-of-plane curvature. This approximation probably explains the scatter in our data points.

So far we have shown that curvature of a *rigid* wall induces forces on the large spheres in binary particle mixtures. To conclude this Letter, we consider theoretically a binary hard-sphere mixture in the presence of *flexible* walls. This extra degree of freedom introduces a competition between depletion and curvature energy that can produce a variety of new phenomena. For example, we expect that under some circumstances, the membrane will spontaneously bend around the large sphere (Fig. 4). We anticipate that these effects will be observable and that understanding this mechanism will be essential to predict the behavior of unilamellar phospholipid vesicles containing particles of different sizes.

The membrane will spontaneously envelop the large sphere only if the resulting total free energy change, ΔF, is negative. Our experiment indicates that the membrane-particle interactions are very short-ranged, so we use the hard-sphere and hard-wall approximations. We therefore divide the full free energy into two terms, one representing the net adhesion induced by the colloidal spheres, the other the vesicle's bending energy: $F = F_{\rm adh} + F_{\rm ves}$.

The experiment described above shows that for rigid membranes, $F_{\rm adh}$ can be well described by the depletion-force model. For flexible membranes we must add a new contribution to $F_{\rm adh}$ to account for the "steric repulsion" effect [18,19]. For $R_S \ll R_L$ we may approximate the latter by the interaction between a flat hard wall and a fluctuating membrane at constant mean separation x. This free energy equals $0.06(k_{\rm B}T)^2/\kappa x^2$ per unit area [20,21]. For unilamellar phospholipid membranes, the bending stiffness $\kappa \approx 15 k_{\rm B}T$ [22]. Approximating the change of excluded volume upon adhesion by $2R_S - x$ per unit area and again taking the small-sphere volume fraction to be $\phi_S = 0.3$, we minimize the total adhesive energy (depletion attraction plus steric repulsion) to find $x \sim 0.5 R_S$ and the adhesive energy $F_{\rm adh} = -0.091 k_{\rm B}T \cdot A^*/{R_S}^2$, where A^* is the area of contact between the membrane and the sphere (Fig. 4(b)) [23].

The vesicle's elastic energy, $F_{\rm ves}$, depends only on the membrane curvature. We neglect the constant-volume and constant-area constraints of a vesicle and instead consider an infinite membrane. Thus the local curvature energy change upon adhesion is just $F_{\rm ves} = 2\kappa A^*/{R_L}^2$ [24,25]. Combining $F_{\rm adh} + F_{\rm ves}$, we see that adhesion and engulfment are favored when $\alpha \equiv R_L/R_S > \sqrt{2\kappa/0.091 k_{\rm B}T} = 18$. A more detailed analysis of the deformation of vesicles at a generically sticky surface, specialized to the case of interest here, gives a similar result [26]. The required regime for α is easily accessible, using either polymers or spheres as the small particles.

In conclusion, we have measured for the first time a curvature-induced entropic force in a system of hard spheres trapped in a rigid vesicle. The results show that the distribution of particles within the vesicle is strongly affected by the local shape of the vesicle wall. Furthermore, a simple estimate predicts shape transitions of unilamellar phospholipid vesicles induced by particles inside the vesicle. The ideas presented here suggest a way to understand several phenomena in cellular interiors and complex fluids inside porous media. For example, in a vesicle whose membrane contains multiple species of lipids, the lipids can segregate into regions with different curvatures [27]. In such a sample, the particle distribution, which depends on curvature, would correlate with the local *composition* of the membrane. This mechanism may provide considerable specificity in associations between macromolecules and lipids. Finally, when the size ratio is more extreme or the vesicle wall is less rigid, the spheres may be able to induce budding and fission of the vesicle.

---

[1] A. D. Dinsmore, A. G. Yodh, and D. J Pine, Phys. Rev. E **52**, 4045 (1995).

[2] A. Imhof and J. K. G. Dhont, Phys. Rev. Lett. **75**, 1662 (1995).

[3] U. Steiner, A. Meller, and J. Stavans, Phys. Rev. Lett. **74**, 4750, (1995).

[4] J. Bibette, D. Roux, and B. Pouligny, J. Phys. II Fr. **2**, 401 (1992).

[5] P. Bartlett and P. N. Pusey, Physica A **194**, 415 (1993).

[6] S. M. Ilett, A. Orrock, W. C. K. Poon, and P. N. Pusey, Phys. Rev. E **51**, 1344 (1995).

[7] P. D. Kaplan, J. L. Rouke, A. G. Yodh, and D. J. Pine, Phys. Rev. Lett. **72**, 582 (1994).

[8] P. D. Kaplan, L. P. Faucheux, and A. J. Libchaber, Phys. Rev. Lett. **73**, 2793 (1994); mixtures of large colloidal spheres and small polymers or micelles: D. L. Sober and J. Y. Walz, Langmuir **11**, 2352 (1995); A. Milling and S. Biggs, J. Colloid Interface Sci. **170**, 604 (1995); Y. N. Ohshima *et al*, Phys. Rev. Lett. **78**, 3963 (1997).

[9] A. D. Dinsmore, A. G. Yodh, and D. J. Pine, Nature **383**, 259 (1996).

[10] A. P. Minton, Biophys. J. **63**, 1090 (1992); Biophys. J. **68**, 1311 (1995).

[11] S. Asakura and F. Oosawa, J. Chem. Phys. **22**, 1255 (1954).

[12] A. Vrij, Pure Appl. Chem. **48**, 471 (1976).

[13] A. D. Dinsmore, A. G. Yodh, P. B. Warren, and W. C. K. Poon, submitted to Europhys. Lett. (1997).

[14] W. C. K. Poon and P. B. Warren, Europhys. Lett. **28**, 513 (1994).

[15] A. D. Dinsmore and A. G. Yodh (to be submitted).
[16] J. C. Crocker and D. G. Grier, Phys. Rev. Lett. **73**, 352 (1994); J. Coll. Interface Sci. **179**, 298 (1996).
[17] R. Dickman, V. Simonian, and P. Attard, (submitted); J. Y. Walz and A. Sharma, J. Coll. Int. Sci. **168**, 485 (1994).
[18] W. Helfrich and R.-M. Servuss, Nuovo Cimento **3D**, 137 (1984).
[19] C. R. Safinya, D. Roux, G. S. Smith, S. K. Sinha, P. Dimon, N. A. Clark, and A. M. Bellocq, Phys. Rev. Lett. **57**, 2718 (1986).
[20] R. Lipowsky and B. Zielinska, Phys. Rev. Lett. **62**, 1572 (1989).
[21] U. Seifert, Adv. Phys. **46**, 13 (1997).
[22] R. Lipowsky, in *The Structure and Dynamics of Membranes*, edited by R. Lipowsky and E. Sackmann, Handbook of Biological Physics Vol. 1B (Elsevier, Amsterdam, 1995); E. Evans and D. Needham, J. Phys. Chem. **91**, 4219 (1987).
[23] For extremely flexible membranes with $\kappa \sim k_{\mathrm{B}}T$ the adhesion is lost completely. Details of this calculation will appear elsewhere.
[24] P. B. Canham, J. Theor. Biol. **26**, 61 (1970).
[25] W. Helfrich, Z. Naturforsch **28c**, 693 (1973).
[26] U. Seifert and R. Lipowsky, Phys. Rev. A **42**, 4768 (1990).
[27] R. Lipowsky, J. Phys. II Fr. **2**, 1825 (1992); E. Sackmann J. Kas, and J. Radler, Physica Scripta **T49**, 111 (1993); U. Seifert, Phys. Rev. Lett **70**, 1335 (1993).

ACKNOWLEDGMENTS

We are happy to thank D. J. Pine, T. C. Lubensky, U. Seifert, D. A. Weitz and J. C. Crocker for their helpful discussions. AGY was supported in part by NSF grant DMR96-23441 and by the NSF-PENN MRSEC Program. PN was supported in part by NSF grant DMR95–07366, and by US/Israeli Binational Foundation grant 94–00190. DTW acknowledges support from the Howard Hughes Medical Institute.

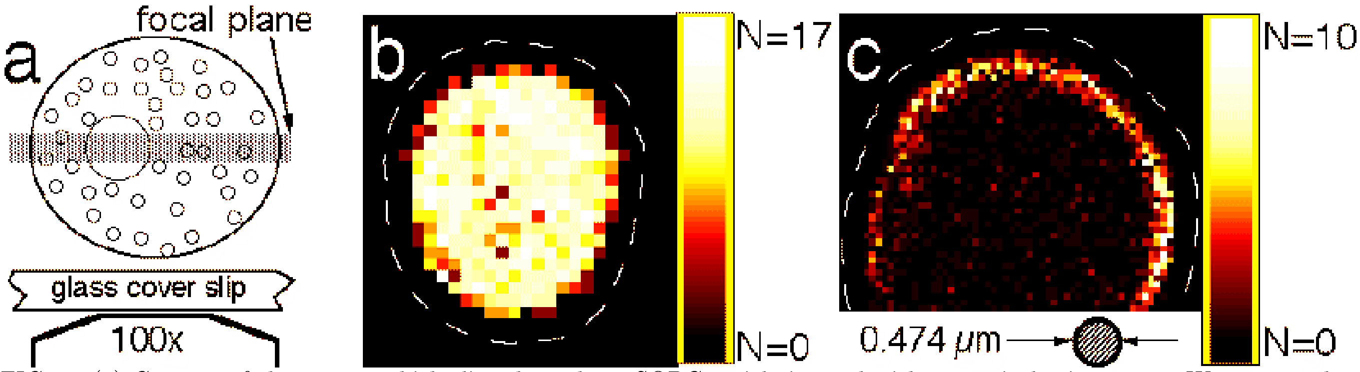

FIG. 1. (a) Cartoon of the 600-nm thick slice through an SOPC vesicle imaged with an optical microscope. We measured the in-plane positions of the larger colloidal sphere when it was in focus. (b)(color) Probability distribution of a single 0.237-μm-radius polystyrene sphere inside a vesicle (no small spheres). The white dashed line is the edge of the vesicle, and the colored points indicate the number of times, N, the center of the sphere was observed in a bin located at a given point. There were 2000 events and the bins were 130 nm x 130 nm. The sphere simply diffused freely throughout all of the available space. (c) (color) Same as in (b), but with a vesicle that also contained small spheres ($\phi_S = 0.30, R_S = 0.042$ μm$, \alpha = 5.7$). There were 2300 events and the bin size was 65 nm. The large sphere was clearly attracted to the vesicle wall, especially where the vesicle was most curved.

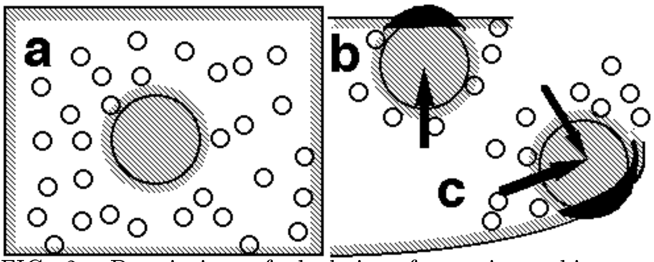

FIG. 2. Description of depletion forces in a binary hard-sphere mixture. The centers of mass of the small spheres are excluded from the hatched regions, within one radius of the surface of the large sphere and of the walls. In (a), the volume accessible to the small-sphere centers, V_{acc} is the total volume minus the hatched regions. (b) When the large sphere moves to the wall, the excluded regions overlap, as shown in black, and V_{acc} increases by this amount. The small spheres' entropy therefore increases. (c) Because of the changing wall curvature, the size of the overlap depends on sphere position. The large sphere will move along the wall to maximize the size of the overlap region, as indicated by the arrow.

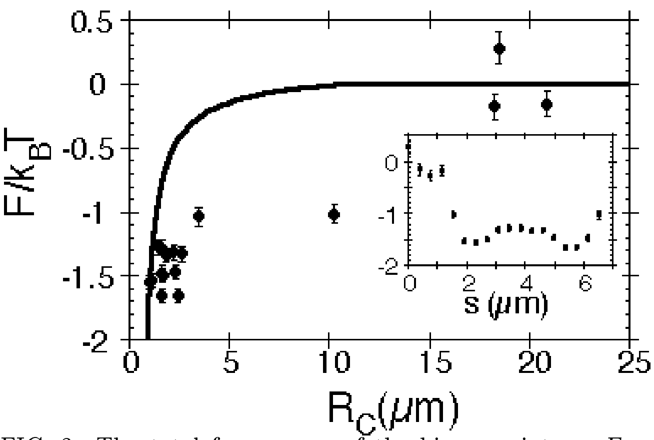

FIG. 3. The total free energy of the binary mixture, F, when the large (0.237-μm) sphere was at the vesicle wall. F is plotted in units of $k_{\mathrm{B}}T$ as a function of the wall curvature radius, R_C. The symbols represent measurements and the line represents the results of the calculation described in the text. (Inset) F/k_BT *vs.* position, s, along the perimeter of the vesicle. The origin (s=0) is located at the lower left of the vesicle shown in Fig. 1(c).

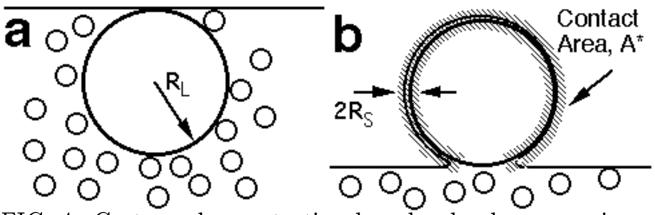

FIG. 4. Cartoon demonstrating how hard spheres can induce a change in shape of a vesicle. (a) When the membrane is flat, the excluded-volume overlap is minimized and the curvature energy is zero. (b) When the vesicle envelops the large sphere, the curvature energy increases, but so does the excluded-volume overlap (hatched region).